

# Electrochemical Quartz Crystal Microbalance Studies of the Rectified Quantized Charging of Gold Nanoparticle Multilayers

Fengjun Deng and Shaowei Chen\*

Department of Chemistry and Biochemistry, University of California, Santa Cruz, California 95064

Received August 3, 2006. In Final Form: October 2, 2006

Electrochemical quartz crystal microbalance (EQCM) was employed to investigate the dynamics of rectified quantized charging of gold nanoparticle multilayers by in situ monitoring of the interfacial mass changes in aqueous solutions with varied electrolytes. EQCM measurements showed that interfacial mass changes only occurred at potentials more positive than the potential of zero charge (PZC), where nanoparticle quantized charging was well-defined, whereas in the negative potential regime where only featureless voltammetric responses were observed, the QCM frequency remained virtually invariant. This was ascribed to the fact that nanoparticle quantized charging was induced by the formation of ion-pairs between hydrophobic electrolyte anions ( $\text{PF}_6^-$ ,  $\text{ClO}_4^-$ ,  $\text{BF}_4^-$ , and  $\text{NO}_3^-$ ) and positively charged gold nanoparticles. Based on the total frequency changes and the number of electrolyte anions adsorbed onto the particle layers, the number of water molecules that were involved in the ion-pairing processes was then quantitatively estimated at varied particle charge states, which was found to increase with increasing hydrophobicity of the anions. Additionally, the electron-transfer dynamics of the gold particle multilayers were also evaluated by electrochemical impedance measurements. It was found that the particle electron-transfer rate was about an order of magnitude slower than that of the ion diffusion and binding.

## Introduction

Several years ago, it was observed that the quantized capacitance charging of monolayer-protected gold nanoparticles could be rectified by simple electrolyte anions of varied degrees of hydrophobicity in aqueous solutions.<sup>1–5</sup> The unique behaviors were interpreted on the basis of the Randle's equivalent circuit where the ion-pair formation between the electrolyte anions and the positively charged particles led to the manipulation of the electrode interfacial double-layer capacitance and hence the voltammetric currents. In addition, it has been found that the number of electrolyte anions bound to the particle is mainly determined by the particle charge state.<sup>2,5</sup> For instance, the ratio between the particle-bound  $\text{PF}_6^-$  ions and the particle charge state was essentially 1:1 for both monolayers and multilayers of gold nanoparticles. However, there has not been any quantitative study of the involvement, if any, of water molecules in these ion-pairing processes. Because of the discrepancy of ion solvation,<sup>6–9</sup> it is anticipated that the ion-pairing interactions will result in the adsorption/desorption of water molecules at the electrode interface during potential sweeping (and hence particle charging). The resulting interfacial mass change should be readily detectable by using electrochemical quartz crystal microbalance (EQCM).

EQCM has been used as a powerful tool in the investigations of interfacial mass change during electrochemical processes.<sup>10–14</sup>

\* Corresponding author. Tel.: (831) 459-5841. Fax: (831) 459-2935. E-mail: schen@chemistry.ucsc.edu.

- (1) Chen, S. W. *J. Am. Chem. Soc.* **2000**, *122*, 7420–7421.
- (2) Chen, S. W.; Pei, R. J. *J. Am. Chem. Soc.* **2001**, *123*, 10607–10615.
- (3) Chen, S. W.; Pei, R. J.; Zhao, T. F.; Dyer, D. J. *J. Phys. Chem. B* **2002**, *106*, 1903–1908.
- (4) Chen, S.; Deng, F. *Proc. SPIE* **2002**, *4807*, 93–99.
- (5) Deng, F. J.; Chen, S. W. *Phys. Chem. Chem. Phys.* **2005**, *7*, 3375–3381.
- (6) Jenkins, H. D. B.; Thakur, K. P. *J. Chem. Educ.* **1979**, *56*, 576–577.
- (7) Stangret, J.; Gampe, T. *J. Phys. Chem. A* **2002**, *106*, 5393–5402.
- (8) Smiechowski, M.; Goflo, E.; Stangret, J. *J. Phys. Chem. B* **2004**, *108*, 15938–15943.
- (9) Marcus, Y. *Ion Solvation*; Wiley: Chichester; New York, 1985.
- (10) Hillman, A. R.; Swann, M. J.; Bruckenstein, S. *J. Phys. Chem.* **1991**, *95*, 3271–3277.
- (11) Schneider, T. W.; Buttry, D. A. *J. Am. Chem. Soc.* **1993**, *115*, 12391–12397.

The fundamental principle is primarily reflected by the Sauerbrey equation, which dictates that the change of the quartz crystal vibrational frequency is directly proportional to the surface mass change.<sup>15</sup> In combination with electrochemical measurements, the in situ approach allows one to correlate the interfacial dynamics with the charge-transfer reactions. For instance, Szucs<sup>16</sup> and Echegoyen<sup>17</sup> have used EQCM to investigate the interfacial cationic fluxes in  $\text{C}_{60}$  thin films. In the present study, we will use EQCM to investigate the interfacial dynamics of the rectified quantized capacitance charging of gold nanoparticle multilayers with a focus on the effects of the nature of electrolyte anions on the particle electron-transfer properties. Our main motivation is to quantify the interfacial mass change arising from the ion-pairing interactions, and thus to advance our understanding of the molecular mechanism that governs the nanoscale interfacial electron transfer.

Specifically, we first fabricate gold nanoparticle multilayers by the dropcast method. The effects of the nature of the electrolyte anions on the interfacial mass change and the particle electron transfer kinetics are then examined by in situ EQCM and electrochemical impedance spectroscopy measurements. It is found that the number of water molecules that are involved in the ion-pairing interactions varies rather sensitively with the hydrophobicity of the electrolyte anions and less so with the particle charge states; in addition, the particle electron-transfer rate is found to be lower than that of ion diffusion and binding and increases somewhat with increasing particle charge state.

## Experimental Section

**Chemicals.** Potassium hexafluorophosphate ( $\text{KPF}_6$ , 99%, ACROS), ammonium hexafluorophosphate ( $\text{NH}_4\text{PF}_6$ , 99%, ACROS), potassium perchlorate ( $\text{KClO}_4$ , ACROS), ammonium perchlorate

- (12) Takada, K.; Diaz, D. J.; Abruna, H. D.; Cuadrado, I.; Casado, C.; Alonso, B.; Moran, M.; Losada, J. *J. Am. Chem. Soc.* **1997**, *119*, 10763–10773.
- (13) Kawaguchi, T.; Yasuda, H.; Shimazu, K.; Porter, M. D. *Langmuir* **2000**, *16*, 9830–9840.
- (14) Cliffel, D. E.; Bard, A. J. *Anal. Chem.* **1998**, *70*, 1993–1998.
- (15) Sauerbrey, G. *Z. Phys.* **1959**, *155*, 206–222.
- (16) Szucs, A.; Novak, M. *J. Solid State Electrochem.* **2005**, *9*, 304–311.
- (17) Song, F.; Echegoyen, L. *J. Phys. Chem. B* **2003**, *107*, 5844–5850.

( $\text{NH}_4\text{ClO}_4$ , 99.8%, ACROS), ammonium tetrafluoroborate ( $\text{NH}_4\text{BF}_4$ , 97%, ACROS), tetra-*n*-octylammonium bromide (98%, Aldrich), 1-hexanethiol (C6SH, 96%, ACROS), 1-butanethiol (C4SH, 98%, ACROS), and sodium borohydride ( $\text{NaBH}_4$ , 98%, ACROS) were all used as received. Potassium nitrate ( $\text{KNO}_3$ , Fisher) and ammonium nitrate ( $\text{NH}_4\text{NO}_3$ , Fisher) were recrystallized twice prior to use. Hydrogen tetrachloroauric acid ( $\text{HAuCl}_4$ ) was synthesized by dissolving ultrahigh purity gold (99.999%, Johnson Matthey) in freshly prepared aqua regia. Water was supplied by a Barnstead Nanopure water system (18.3 M $\Omega$ ). All solvents were purchased from typical commercial sources and used as received.

**Particle Synthesis.** 1-Hexanethiolate-protected gold nanoparticles (C6Au) were synthesized by using the modified Brust reaction<sup>18</sup> followed by fractionation and thermal annealing to reduce the core size dispersity of the gold particles. The fraction with core diameter of ca. 2.0 nm (as determined by transmission electron microscopic measurements) was used in the subsequent measurements.

**Preparation of Gold Nanoparticles Multilayers.** Particle assemblies were prepared by dropcasting an aliquot of a particle solution onto a quartz crystal surface. The quartz crystals (International Crystal Manufacturing) were made from polished quartz plates with a resonant frequency of 8 MHz and a crystal diameter of 14 mm. A 10 nm layer of Cr was first deposited onto the center of the quartz crystals (diameter 5 mm) as the adhesion layer, followed by 100 nm of gold. First, the QCM crystal was washed with ethanol, and blow-dried with a gentle stream of ultrahigh purity nitrogen. The dried QCM crystal was then cleaned in a UVO cleaner (model 42, Jelight Co.) for 15 min. Gold nanoparticle multilayers were fabricated by dropcasting a calculated amount of C6Au particles (dissolved in dichloromethane) onto the QCM gold surface with a Hamilton microliter syringe. The QCM was then dried in a  $\text{N}_2$  stream again. The QCM frequency before and after particle deposition was monitored in air, and the total mass of the gold particles on the QCM surface was calculated by using the Sauerbrey equation.<sup>15</sup>

**Electrochemistry and EQCM Measurements.** Electrochemical experiments were carried out with a CHI 440 electrochemical workstation with a time-resolve quartz crystal microbalance. The QCM crystal (with the particle layers prepared above) was used as the working electrode, an Ag/AgCl wire was used as the quasi-reference electrode, and the counter electrode was a Pt coil. Electrochemical impedance experiments were carried out by using an EG&G PARC 273 potentiostat/galvanostat and a Frequency Detection Analyzer (model 1025).

## Results and Discussion

**Rectified Quantized Charging.** Figure 1 shows the representative cyclic (panel A, CV) and differential pulse voltammograms (panel B, DPV) of a dropcast C6Au multilayer on a QCM gold electrode surface in various aqueous electrolytes. Within the potential range of  $-0.2$  to  $+0.6$  (V vs Ag/AgCl), a series of well-defined voltammetric peaks emerged, which were attributed to the quantized charging to the surface-bound gold nanoparticles, whereas at negative potentials, only featureless responses were observed. Such unique behaviors have been ascribed to the ion-induced rectification of the particle single electron transfers.<sup>1-5</sup> As reported previously, the onset potentials shifted cathodically with increasing hydrophobicity of the electrolyte anions,  $\text{PF}_6^- \rightarrow \text{ClO}_4^- \rightarrow \text{BF}_4^- \rightarrow \text{NO}_3^-$ , akin to the effect of anion-specific adsorption on the negative shift of electrode potential of zero charge.<sup>19</sup>

The surface coverage (number of layers) of gold nanoparticles on the QCM surface was then estimated by two methods. The first is based on the variation of the voltammetric peak currents with potential sweep rate. From Figure 1 (panel C), we can see that the variation of the first anodic peak current with potential

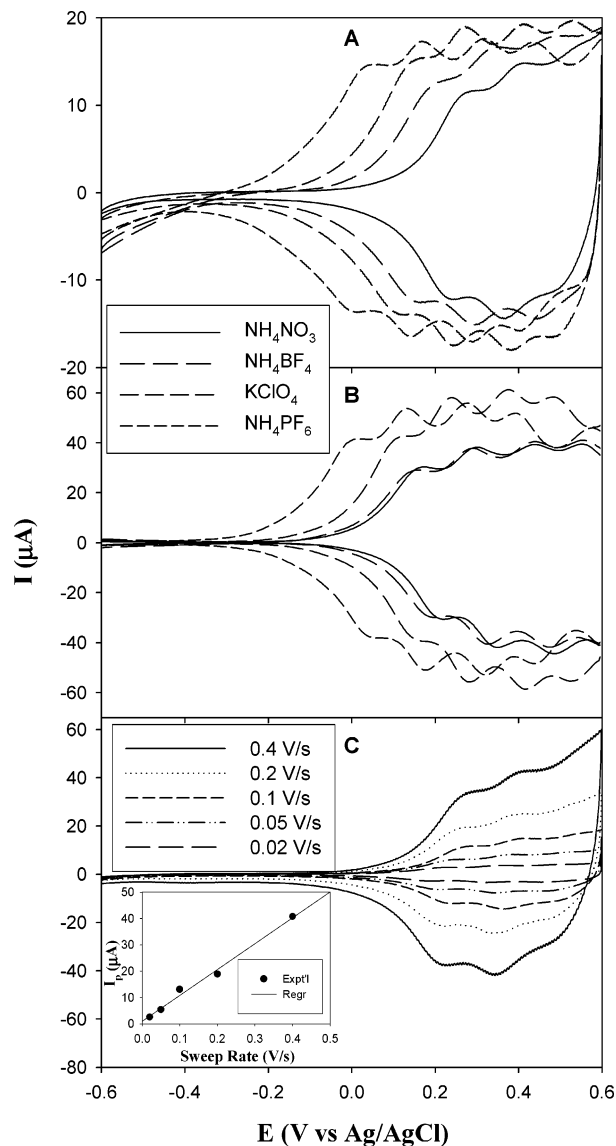


**Figure 1.** Cyclic (panel A, CV) and differential pulse voltammograms (panel B, DPV) of a C6Au multilayer self-assembled onto a gold electrode surface in various aqueous electrolytes (0.1 M):  $\text{NH}_4\text{NO}_3$ ,  $\text{NH}_4\text{BF}_4$ ,  $\text{KClO}_4$ , and  $\text{KPF}_6$ . In (A), potential sweep rate  $100 \text{ mV s}^{-1}$ ; and in (B), DC ramp  $4 \text{ mV s}^{-1}$ , pulse amplitude  $50 \text{ mV}$ . Panel C depicts the CVs in  $0.1 \text{ M NH}_4\text{NO}_3$  at different scan rates, which are shown as figure legends. The inset shows the variation of the peak current of the first charging step with potential scan rate, where symbols are experimental data and line is the linear regression.

sweep rate exhibits a very good linear relationship. This is consistent with a surface confined system.<sup>19</sup> From the slope (inset), one can estimate the surface coverage of this particle assembly,  $5.36 \times 10^{-10} \text{ mol/cm}^2$ , corresponding to about 16.2 layers of particles (the coverage for a single monolayer of particles is ca.  $3.30 \times 10^{-11} \text{ mol/cm}^2$  by assuming a fully intercalated nanoparticle assembly). The particle surface coverage can also be estimated from QCM measurement. According to the Sauerbrey equation (eq 1),<sup>15</sup> the change in frequency ( $\Delta f$ ) directly reflects the interfacial mass change on the QCM surface,

$$\Delta m = -\frac{\sqrt{\rho_q \mu_q} \Delta f}{2f_0^2} \quad (1)$$

where  $f_0$  is the resonant frequency of the quartz crystal (8 MHz in the present case),  $\rho_q$  is the density of quartz ( $2648 \text{ kg/m}^3$ ), and

(18) Brust, M.; Walker, M.; Bethell, D.; Schiffrin, D. J.; Whyman, R. *J. Chem. Soc., Chem. Commun.* **1994**, 801–802.

(19) Bard, A. J.; Faulkner, L. R. *Electrochemical Methods: Fundamentals and Applications*, 2nd ed.; John Wiley: New York, 2001.

**Table 1. Number of C6Au Particle Layers Estimated from Electrochemical and QCM Measurements**

electrochemical coverage <sup>a</sup>	1.3	2.2	3.1	12.5	14.1	16.2	5.7	7.9	4.2
QCM coverage <sup>b</sup>	42.4	15.7	20.7	28.9	35.9	31.9	10.2	12.4	5.8
ratio ( <i>R</i> ) of electrochemical/QCM layers	0.03	0.14	0.15	0.36	0.39	0.51	0.56	0.64	0.72

<sup>a</sup> Estimated from CV measurements carried out in 0.1 M KNO<sub>3</sub> (e.g., Figure 1). <sup>b</sup> Calculated from QCM frequency change measured in air.

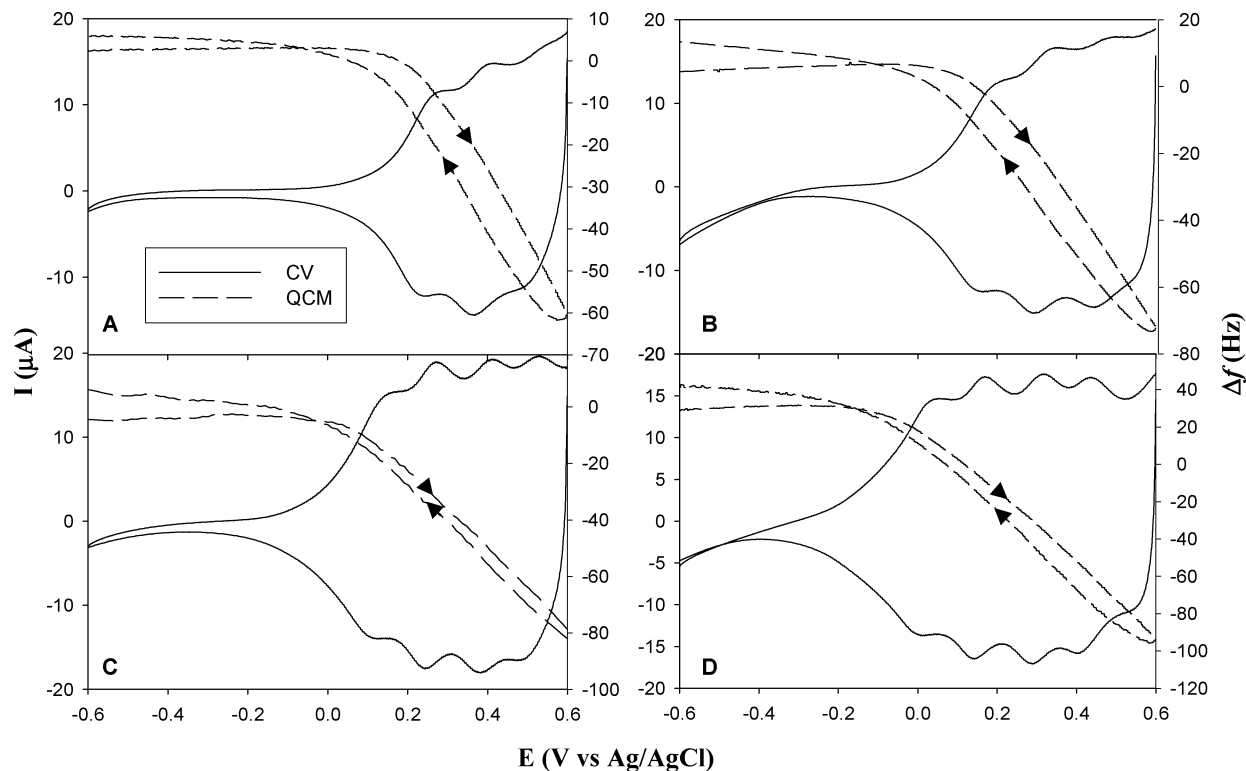


**Figure 2.** Cyclic voltammograms and in situ QCM frequency change of a C6Au multilayer in various aqueous solutions (0.1 M): (A) KNO<sub>3</sub>, (B) NH<sub>4</sub>BF<sub>4</sub>, (C) KClO<sub>4</sub>, and (D) KPF<sub>6</sub>. Potential scan rate 100 mV/s.

$\mu_q$  is its shear modulus ( $2.947 \times 10^{10} \text{ kg m}^{-1} \text{ s}^{-2}$  for AT-cut quartz crystals). From the frequency change (8225 Hz, measured in air), the surface coverage of the gold particles is calculated to be  $1.05 \times 10^{-9} \text{ mol/cm}^2$ , corresponding to 31.9 layers of particles deposited on the QCM surface, which is substantially greater than the electrochemical value estimated above.

Table 1 summarizes the results of gold nanoparticle surface coverage in a series of preparations. From Table 1, we can see that the particle surface coverage calculated from voltammetric measurements is generally smaller than that estimated from the QCM results, suggesting that not all particles in the multilayer films are electrochemically accessible and active. Also, there is no clear correlation between these two measurements, which may be attributable to the random nature of the preparation method of the particle films. For instance, the fraction (*R*) of particles that are electrochemically active varies from 0.03 to 0.72 when the effective (QCM) particle coverage ranges from 3 to 42 layers. Because the voltammetric responses arise from ion-pairing between surface-immobilized nanoparticles and electrolyte anions, the above studies suggest that anion penetration (and hence ion-pairing) most probably only occurs at the top few layers of the particle films. These phenomena are in contrast to particle porous multilayer films in organic solutions where entire multilayer films were found to be electrochemically accessible.<sup>20,21</sup> To maximize the voltammetric current responses, we will limit the subsequent studies to those particle films with at least 50% particles electrochemically active.

For each particle assembly, the electrochemical coverage was found to be virtually independent of the electrolyte anions, suggesting similar penetration properties in the particle films. While the top layers of particles contribute to the quantized charging currents, the interior particles most probably serve as the structural matrixes to relay the electron transfer to the electrode surface. Because the electron transfer within the C6Au particle solids of different charge states is of the order of  $10^6$ – $10^8 \text{ s}^{-1}$ ,<sup>21</sup> the overall electron-transfer kinetics is anticipated to be dominated by the rectified quantized charging process at the top layers, which is several orders of magnitude slower (vide infra).

**Interfacial Mass Change.** The measurements of the interfacial mass change during the rectified quantized charging of the gold particle multilayers show further experimental evidence to support the ion-pairing mechanism. Figure 2 shows the cyclic voltammograms (—) and the frequency change (---) of the same C6Au layer as that used in Figure 1 in varied aqueous solutions (0.1 M): (A) KNO<sub>3</sub>; (B) NH<sub>4</sub>BF<sub>4</sub>; (C) KClO<sub>4</sub>; and (D) KPF<sub>6</sub>. From Figure 2, one can see that, in the negative potential regime between  $-0.6 \text{ V}$  and the onset potential, the QCM frequencies remained virtually invariant and the currents were featureless, suggesting that there was essentially no mass change at the electrode interface in this potential regime. By contrast, at more

(20) Gittins, D. I.; Bethell, D.; Nichols, R. J.; Schiffrin, D. J. *J. Mater. Chem.* **2000**, *10*, 79–83.

(21) Hicks, J. F.; Zamborini, F. P.; Osisek, A.; Murray, R. W. *J. Am. Chem. Soc.* **2001**, *123*, 7048–7053.

positive potentials where nanoparticle quantized charging was very well-defined and the currents were substantially greater, the frequency decreased rather significantly during the anodic scan and recovered almost completely in the reverse scan. This can be attributed to the reversible interfacial mass change as a result of the formation and subsequent dissociation of ion-pairing between the electrolyte anions and gold nanoparticles. In the anodic scan, the anions were absorbed to the particle layer forming ion-pairs with the positively charged particles, and in the cathodic scan, the anions were repelled from the particle layer resulting in interfacial mass loss.

The strength of the ion-pairing interactions is determined by the nature of the electrolyte anion and the nanoparticle charge states. To quantify the ion-pairing interactions between electrolyte anions and surface-immobilized nanoparticles, we varied the concentration of the anions and measured the corresponding voltammetric responses, as the particle peak potentials were anticipated to shift cathodically with increasing anion concentration,<sup>1–5</sup>

$$E_f = E^{0'} + \frac{RT}{n_a F} \ln \frac{K_2}{K_1} - (p - q) \frac{RT}{n_a F} \ln [\text{anion}] \quad (2)$$

where  $E_f$  and  $E^{0'}$  are the formal potential in the presence and absence of ion-pairing,  $n_a$  is the (effective) number of electron transfer, and  $K_1$  and  $q$  ( $K_2$  and  $p$ ) are the equilibrium constant and the number of anions bound to the reduced (oxidized) forms of the particle, respectively. Figure 3A shows the representative DPV of the C6Au multilayer in aqueous solutions containing varied concentrations of  $\text{NH}_4\text{BF}_4$  (with the addition of KAc at an appropriate concentration to maintain the solution ionic strength constant at 0.1 M). One can see that indeed with increasing concentration of  $\text{NH}_4\text{BF}_4$ , the overall voltammetric profiles shifted cathodically, as anticipated from eq 2. Figure 3B exhibits the variation of the formal potentials of the particle quantized charging at four different charge states with the natural logarithm of  $\text{NH}_4\text{BF}_4$  concentration, where symbols are experimental data, and lines are linear regressions. From panel B, we can see good linearity for the four charging steps within the concentration range of 0.02–0.08 M. The corresponding slopes are  $-32.3$  mV ( $z = +1/0$ ),  $-33.3$  mV ( $z = +2/+1$ ), and  $-55.7$  mV ( $z = +3/+2$ ), respectively. If one assumes that at zero charge state, no ion-pairing occurs, then the numbers of  $\text{BF}_4^-$  anions bound to the particles at varied charge states can be estimated to be ca. 1.4 ( $z = +1/0$ ), 2.4 ( $z = +2/+1$ ), and 3.5 ( $z = +3/+2$ ).

Similar measurements were carried out with other electrolyte solutions. Table 2 summarizes the number of electrolyte anions bound to the particles at varied particle charge states. We can see that, overall, the behaviors for the  $\text{PF}_6^-$ ,  $\text{ClO}_4^-$ , and  $\text{BF}_4^-$  anions are rather similar. They are close to the values expected for a 1:1 binding ratio, consistent with previous research results with particle organized assemblies.<sup>2–5</sup> For instance, for  $\text{PF}_6^-$ , the number of ions bound to the particles at different charge state is 0.9 ( $z = +1/0$ ), 2.1 ( $z = +2/+1$ ), and 3.8 ( $z = +3/+2$ ). For  $\text{NO}_3^-$  ions, overall the numbers of particle-bound anions are larger than those for the other three anions. Such a discrepancy most probably arises from the difference in solvation structures, as the more hydrophilic and better solvated nitrate is anticipated to exhibit weaker ion-pairing interactions with the particles.

From the above measurements, it is anticipated that the formation and dissociation of the ion-pairs will lead to mass change at the electrode surface. However, the adsorption/desorption of electrolyte anions alone cannot account for the total interfacial mass change ( $\Delta m$ ) as manifested in QCM

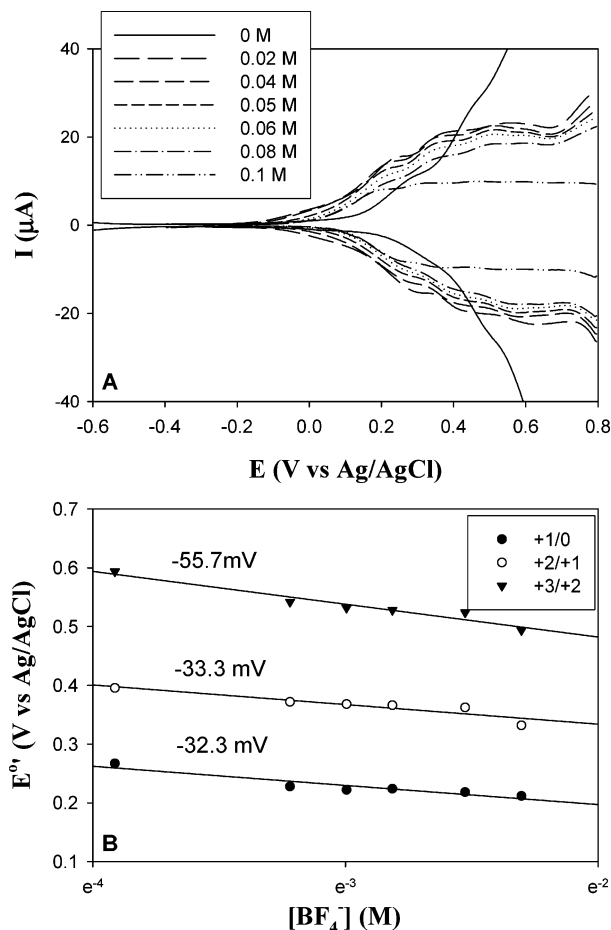


**Figure 3.** Differential pulse voltammograms (A, DPV) of the C6Au multilayer on a QCM electrode surface in aqueous solutions with varied concentrations of KAc and  $\text{NH}_4\text{BF}_4$ . Legends denote the molar concentration of  $\text{NH}_4\text{BF}_4$  with the total electrolyte concentration kept at 0.1 M. (B) Variation of the formal potentials of the first three charging peaks with  $\text{NH}_4\text{BF}_4$  concentration. Symbols are experimental data, and lines are linear regressions. The slopes of the respective linear regression are also shown in the figure.

**Table 2. Number ( $n_a$ ) of Anions Bound to C6Au Particles at Different Particle Charge States**

anions	particle charge state		
	+1/0	+2/+1	+3/+2
$\text{NO}_3^-$	2.3	3.5	4.7
$\text{BF}_4^-$	1.4	2.4	3.5
$\text{ClO}_4^-$	0.5	1.4	2.1
$\text{PF}_6^-$	0.9	2.1	3.8

frequency measurements. It is most likely that additional contributions arise from the loss or gain of water molecules as a result of the varied degree of ion solvation (hydrophobicity), that is,

$$\Delta m = \Delta m_{\text{ai}} + \Delta m_{\text{aq}} \quad (3)$$

where  $\Delta m_{\text{ai}}$  is the mass change due to anions that form ion-pairs with the particles, and  $\Delta m_{\text{aq}}$  is the mass change arising from  $\text{H}_2\text{O}$  molecules involved in the ion-pairing interactions. Figure 4 shows the number of water molecules involved in the interfacial ion-pairing dynamics at varied particle charge state. This is normalized to the number of gold particles that are electrochemically accessible and active. There are several aspects that warrant attention. First, it can be seen that there is a net loss (gain) of water molecules at the electrode interface in the anodic (cathodic)

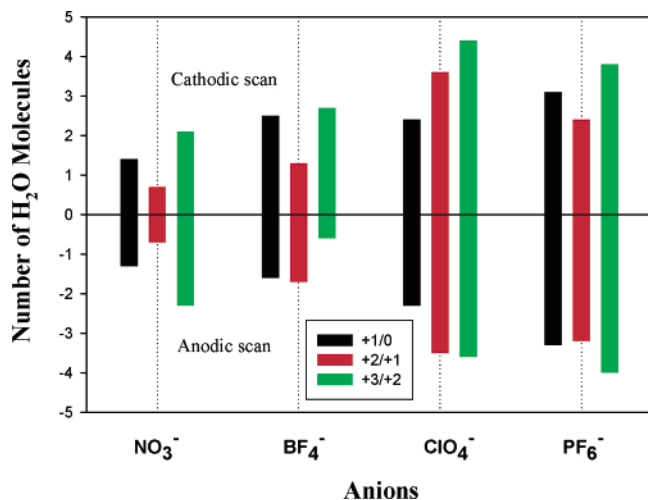


**Figure 4.** The number of water molecules involved in the interfacial dynamics of ion-pairing interactions in the particle quantized charging processes. Data were calculated from the QCM measurements as represented in Figure 2 and normalized to the number of electrochemically active nanoparticles.

scan, concurrently with the adsorption (desorption) of electrolyte anions to (from) the particle surface. This provides strong supporting evidence of the proposed ion-pairing mechanism that results in the manipulation of the electrode interfacial double-layer capacitance (based on the Randle's equivalent circuit) and hence the rectification of the nanoparticle quantized charging, as discussed previously.<sup>1-5</sup> Second, in most cases, the number of water molecules that was desorbed in the forward scan is very close to that of water molecules adsorbed in the reverse scan in all electrolyte solutions under study, indicative of the reversible and rapid nature of the ion-pairing interactions. Third, the numbers of water molecules involved in the interfacial dynamics in the presence of the PF<sub>6</sub><sup>-</sup> and ClO<sub>4</sub><sup>-</sup> ions are generally greater than those in solutions containing the BF<sub>4</sub><sup>-</sup> and NO<sub>3</sub><sup>-</sup> anions at the three particle charge states under study. Of these, PF<sub>6</sub><sup>-</sup> ions have been known to be the most hydrophobic, and consequently the ion-pairing with the particles leads to the most drastic disruption of the interfacial water structure, with ca. 4 water molecules involved in the ion-pairing interactions, whereas only 1–2 water molecules were involved in the case of NO<sub>3</sub><sup>-</sup>. In the presence of ClO<sub>4</sub><sup>-</sup> and BF<sub>4</sub><sup>-</sup>, the data are in the intermediate range. Such an observation is most likely a consequence of the discrepancy of the hydrophobicity (hydration) of these anions, as demonstrated previously in FTIR studies of partially deuterized water in the presence of varied electrolytes.<sup>7,8</sup> At higher charge states, the difference is somewhat less pronounced, possibly because of the enhanced contributions of the electrostatic interactions.

**Electron-Transfer Kinetics.** As reported previously,<sup>1-5</sup> the quantized charging features of nanoparticle organized assemblies in aqueous solutions are interpreted on the basis of the Randle's equivalent circuit. Here, by using electrochemical impedance spectroscopy, we evaluate the electron-transfer kinetics of the C6Au particle multilayers in varied electrolyte solutions. Figure 5 shows two representative Bode plots of the experimental data (symbols) with potential equal to the formal potential of the first charging peak (panel A) and the PZC (panel B), respectively. From Figure 5, one can see that the overall impedance is substantially reduced when the electrode potential moves from PZC to more positive potentials. This is consistent with the appearance of the particle quantized charging features and the significantly greater voltammetric currents at positive potentials (e.g., Figure 1), suggesting that the ion-pairing facilitates the electron transfer of the nanoparticle molecules.

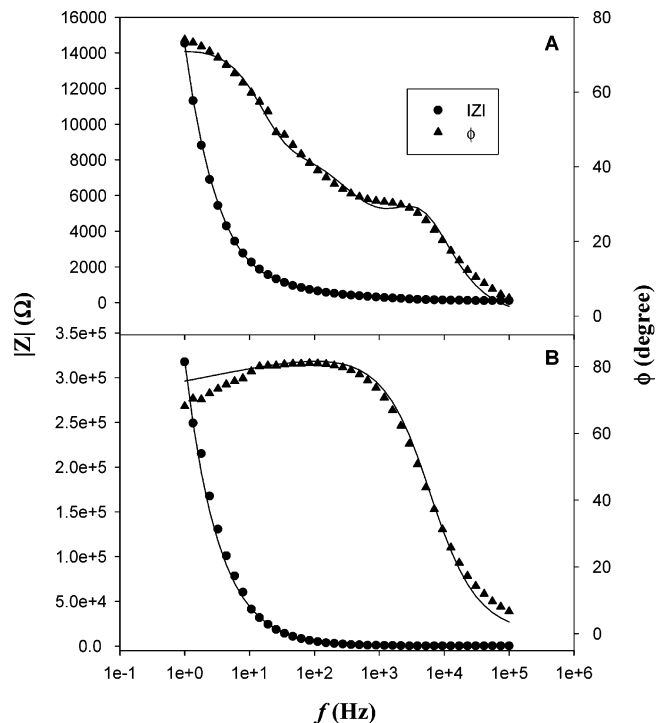
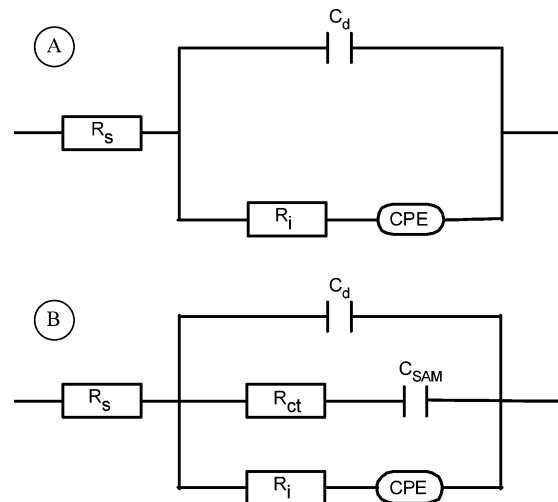


**Figure 5.** Representative Bode plots of the dropcast C6Au multilayer in 0.1 M NH<sub>4</sub>NO<sub>3</sub> at different electrode potentials: (A)  $E = E_{+1/0}'$  and (B)  $E = \text{PZC}$ . Symbols are the experimental data, and lines are the fits by the equivalent circuits shown in Scheme 1.

**Scheme 1. Equivalent Circuits for the Particle Surface Assemblies at Varied Electrode Potentials: (A)  $E \leq \text{PZC}$  and (B)  $E > \text{PZC}$ <sup>a</sup>**



<sup>a</sup>  $R_S$  is the solution resistance;  $C_{EL}$  is the double-layer capacitance at the part of the electrode surface that is not covered by particles;  $R_i$  is the resistance of the ingress/egress of ions into/out of the particle surface assemblies; CPE is a constant phase element ( $Q$ ) that represents the capacitive property of the particle layers;  $C_{SAM}$  is the collective capacitance of the particles that are electrochemically accessible and active; and  $R_{CT}$  is the particle charge-transfer resistance.

To evaluate the particle charge-transfer kinetics, two equivalent circuits are proposed to model the electrochemical system at different potentials, (A)  $E \leq \text{PZC}$  and (B)  $E > \text{PZC}$ , as depicted in Scheme 1. In the negative potential regime ( $E \leq \text{PZC}$ ), no faradaic current was observed as the ion-pair formation was not favored. In the equivalent circuit (Scheme 1A),  $R_S$  is the solution resistance,  $C_d$  is the double-layer capacitance at the part of the electrode surface that is not covered with particles,  $R_i$  is the resistance of ion ingress into/egress out of the particle

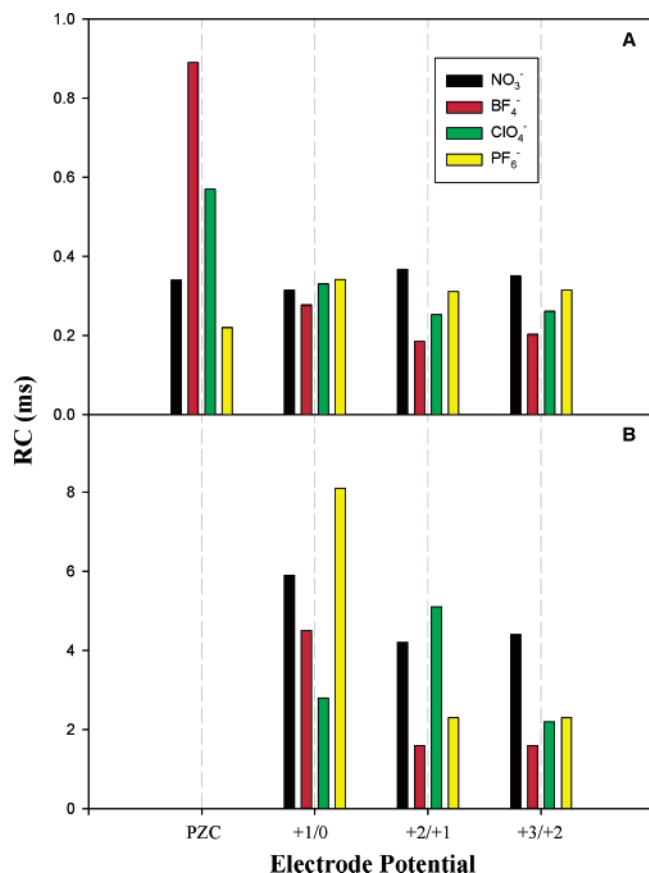


**Figure 6.** RC constants of the ion-pairing (panel A) and electron-transfer reaction (panel B) of the C6Au particle multilayers at different electrode potentials and in varied electrolyte solutions. Data are acquired from the fitting of the impedance spectra as represented in Figure 5 by the equivalent circuits in Scheme 1.

surface assemblies, and CPE is a constant phase element ( $Q$ ) that represents the capacitive property of the particle ensemble. Such a circuit is similar to those used to represent the porous structures in, for instance, electro-corrosion studies.<sup>22</sup> At more positive potentials ( $E > PZC$ ), the ion-pair formation between the anions and gold particles leads to the rectified quantized charging through the immobilized gold nanoparticles. The corresponding equivalent circuit is depicted in panel B with an additional branch to account for the faradaic reactions of the particles, that is,  $R_{ct}$  for particle charge-transfer resistance and  $C_{SAM}$  for the collective capacitance of the electrochemically accessible and active particles. The corresponding fitting curves based on these two equivalent circuits are shown in Figure 5 (lines), where it can be seen that the simulation data are in excellent agreement with the experiment data. From the fittings, one can then evaluate the kinetics of the ion-pairing and electron-transfer processes by the corresponding RC constants.

Figure 6 depicts the time constants for the  $R_iQ$  (A) and  $R_{ct}C_{SAM}$  (B) branches at different electrode potentials and in varied

electrolyte solutions. These time constants can be exploited to evaluate the rates of ion-pairing and particle faradaic reactions, respectively. First, one can see that the time constants for the ion diffusion and pairing process ( $\sim 0.4$  ms) are at least an order of magnitude smaller than that of the particle charge-transfer reaction ( $\sim 4$  ms), indicating that the rate-determining step is the particle faradaic reaction. Second, the ion diffusion and pairing dynamics exhibit only very subtle variation with the nature of the ions and the particle charge state, which suggests similar ion penetration into the particle layers. This is consistent with the voltammetric measurements where the electrochemical surface coverage of the particles is found to be practically independent of the identity of the anions (Figure 1, *vide ante*). By contrast, the particle charge-transfer process appears to be somewhat facilitated at increasing electrode potentials, but with no regular variation with the nature of the electrolyte anions.

It should be noted that, in these particle multilayer films, nanoparticle quantized charging occurs only at the top few layers because of the ion-pairing interactions with electrolyte anions (*vide ante*). The electrons are then relayed to the electrode surface by a hopping mechanism across the interior particle matrix, which has been found to exhibit significantly faster electron-transfer rate constants.<sup>21</sup> Consequently, the overall electron-transfer rates are determined by the particle faradaic process. It is therefore anticipated that the corresponding RC constants should be independent of the thickness of particle films, which has indeed been observed experimentally (not shown). By contrast, the time constants for the ion-pairing process were found to increase with increasing thickness of the particle layers, suggesting impeded penetration of the ions into the particle layers.

## Conclusion

Further mechanistic insights into the interfacial dynamics of the rectified quantized charging of gold nanoparticle surface assemblies have been obtained by EQCM measurements, which in situ monitor the interfacial mass change along with the voltammetric responses. Interfacial mass change was found to occur only at positive electrode potentials where particle quantized charging was well-defined, whereas in the negative potential regime with featureless voltammetric responses, no mass change was found. The total mass change was ascribed to the adsorption/desorption of electrolyte anions to/from the particle layers and to the loss/gain of water molecules that were involved in the ion solvation. The number of water molecules involved in such interfacial dynamics was found to increase with the increasing hydrophobicity of the electrolyte anions. In electrochemical impedance measurements, the kinetics of the ion-pairing and the electron-transfer processes were evaluated. It was found that the former was at least an order of magnitude faster than the latter, indicating that the overall rate-determining step was indeed the particle faradaic reactions.

**Acknowledgment.** This work was supported in part by the NSF (CAREER Award CHE-0456130), ACS-PRF (39729-AC5M), and UCSC.

LA0622976

(22) Cao, C.; Zhang, J. *Introduction to Electrochemical Impedance Spectroscopy*; Science Press: Beijing, 2004.